Topics in Catalysis (2021) 64:1030–1040
https://doi.org/10.1007/s11244-021-01431-2

ORIGINAL PAPER

Water and Carbon Dioxide Adsorption on CaO(001) Studied via Single Crystal Adsorption Calorimetry

J. Seifert[1] · S. J. Carey[1] · S. Schauermann[2] · S. Shaikhutdinov[1] · H.-J. Freund[1]

Accepted: 24 March 2021 / Published online: 15 April 2021

Abstract
A new method to analyze microcalorimetry data was employed to study the adsorption energies and sticking probabilities of D_2O and CO_2 on CaO(001) at several temperatures. This method deconvolutes the line shapes of the heat detector response into an instrument response function and exponential decay functions, which correspond to the desorption of distinct surface species. This allows for a thorough analysis of the adsorption, dissociation, and desorption processes that occur during our microcalorimetry experiments. Our microcalorimetry results, show that D_2O adsorbs initially with an adsorption energy of 85–90 kJ/mol at temperatures ranging from 120 to 300 K, consistent with prior spectroscopic studies that indicate dissociation. This adsorption energy decreases with increasing coverage until either D_2O multilayers are formed at low temperatures (120 K) or the surface is saturated (> 150 K). Artificially producing defects on the surface by sputtering prior to dosing D_2O sharply increases this adsorption energy, but these defects may be healed after annealing the surface to 1300 K. CO_2 adsorbs on CaO(001) with an initial adsorption energy of ~ 125 kJ/mol, and decreases until the saturation coverage is reached, which is a function of surface temperature. The results showed that pre-adsorbed water blocks adsorption sites, lowers the saturation coverage, and lowers the measured adsorption energy of CO_2. The calorimetry data further adds to our understanding of D_2O and CO_2 adsorption on oxide surfaces.

1 Introduction

The interaction of carbon dioxide (CO_2) with surfaces is of key importance in a variety of industrial and environmental applications such as methanol synthesis, exhaust cleaning, and CO_2 capturing [1–5]. CO_2, with respect to its use as a source of carbon in catalytic processes has received massive attention, as the world is addressing issues in climate change, in particular with respect to hydrogenation. The reduction of CO_2 into value-added chemical products is considered to have the most potential for chemical transformation of CO_2 [6–8]. A group at Imperial Chemical Industries (ICI) in Billingham during the 1980s has shown that CO_2 plays an important role in methanol syntheses from $CO/CO_2/H_2$ gas mixtures over a $Cu/ZnO/Al_2O_3$ catalyst. Michael S. Spencer was among those who demonstrated through a careful mechanistic study, using isotopically labelled CO_2, that the mechanism involves the formation of a surface carbonate, its reduction to formate and further on to methanol [9].

Therefore, it is important to understand the interaction of CO_2 with surfaces and specifically oxide surfaces, as they are used as supports and modifiers in catalysis. Here, we report on a study of the interaction of CO_2 with a simple oxide surface, i.e. CaO(001), as well as its interaction with water, which is often present in the CO_2 reaction mixtures. Among alkaline-earth oxides used in such processes, calcium oxide (CaO) often exhibits a higher activity due to a more delocalized electron distribution across surface oxygen atoms compared to other simple oxides [10].

We have recently studied the interaction of CO_2 and water with CaO(001), applying a number of techniques like infrared reflection–absorption spectroscopy (IRAS), scanning tunneling microscopy (STM), and temperature programmed desorption (TPD), in combination with density functional theory (DFT) calculations.[11–13] In particular, at low coverages, CO_2 was found to adsorb strongly (desorption temperature about 450 K) as monodentate carbonates (CO_3^{2-}). However, adsorption becomes even stronger in the presence of water, which readily dissociates on the surface forming

✉ S. J. Carey
carey@fhi-berlin.mpg.de

[1] Fritz-Haber-Institut, Max-Planck-Gesellschaft, Faradayweg 4-6, 14195 Berlin, Germany

[2] Institut für Physikalische Chemie, Christian-Albrechts-Universität zu Kiel, Max-Eyth-Str. 2, 24118 Kiel, Germany

hydroxyls. Surface hydroxyls seem to only affect the adsorption geometry of the carbonates rather than form bicarbonate species. In any case, hydroxyls show a stabilizing effect on CO_2 binding to the CaO surface. It is important to know adsorption energies, so a direct comparison with calculated stabilities may be carried out.

In this connection, the central technique in the present study is microcalorimetry, and the associated data evaluation. For a typical single crystal adsorption calorimetry experiment [14, 15], the heat release for a molecular beam pulse is derived from comparison of the slope of the initial steep rise [16], or the absolute peak height [17–19] of the heat detector's signal in comparison with the corresponding value for a laser reference pulse. This procedure requires that the line shape for molecular beam and laser pulse measurements are congruent. There are several examples in the literature where differences, namely narrowing or broadening of the peak width, have been observed. They have been attributed to kinetically delayed adsorption [20], dissociation [21–23], or desorption of molecules or atoms. It was demonstrated that from deconvolution and convolution of line shapes with exponential decay functions, quantitative information on adsorption kinetics can be derived. Here, we employ a new method of a deconvolution analysis to model the effects of desorption processes on the heat detector signal.

2 Experimental

Microcalorimetry experiments were performed in a UHV (base pressure $< 2 \times 10^{-10}$ mbar) setup equipped with low-energy electron diffraction (LEED), Auger Electron Spectroscopy (AES), a Quadrupole Mass Spectrometer (QMS), and a single-crystal adsorption calorimeter (SCAC) [19]. Briefly, an effusive, doubly differentially pumped multichannel array was used to produce a molecular beam of D_2O water or CO_2. A chopper cut this beam into pulses 266 ms in length. The heat of adsorption was measured with a heat detector consisting of a 9 µm-thick pyroelectric ribbon (β-polyvinylidene fluoride) coated with Au on both sides and calibrated with pulses of HeNe laser light (l = 632.8 nm, 5 mW). Simultaneously, the fraction of molecules that adsorb in a single pulse (i.e., the sticking probability) was measured by the modified King–Wells method [24] with a non-line-of-sight QMS. Deuterated water is used, as opposed to nondeuterated water, to prevent interference of background water with the QMS baseline [12], which greatly improves signal-to-noise in the mass spectrometer data.

The crystalline CaO(001) films were grown on Pt(001) as described elsewhere [25]. Clean Pt(001) surfaces were first prepared by cycles of Ar + sputtering and UHV annealing at high temperatures. Carbon contaminations were removed by annealing in 10^{-7} mbar of oxygen at ~ 700 K followed by thermal flash in UHV to 1000 K. The cleanliness of the Pt metal substrate was inspected by LEED showing the well-documented Pt(001)-"hex" diffraction pattern, which is characteristic of a clean Pt(001) surface. Then Ca was deposited in 5×10^{-7} mbar O_2 at 300 K, followed by UHV annealing at ~ 1200 K for 5 min. The resulting CaO(001) films showed good crystallinity as judged by LEED. The nominal film thickness (> 5 nm) was determined by attenuation of the substrate signals in AES. [12]

3 Deconvolution Analysis for SCAC

For the energy calibration of SCAC experiments, the detector signal for molecular beam pulses is compared with the corresponding signal for a laser pulse. This requires the same temporal and spatial distribution on the sample for the molecular beam and laser which is guaranteed by the same pathways passing apertures and chopper [19, 21]. However, heat release for molecular adsorption may not be as instantaneous as compared to laser irradiation and consequently the line shapes of the heat detector may differ. [16, 20–23, 26]

Figure 1a shows the heat detector signals for the laser and water adsorption on the CaO(001) surface. The molecular beam pulses have been averaged for a number of consecutive pulses and therefore, the shown curves correspond to increasing water coverages. While for the initial ten pulses the signal is identical to the (scaled) laser line shape, it deviates not only with respect to its intensity, but also to its shape and position of maxima and minima for higher water dosages. Thus, simple analysis of peak heights or initial slope may result in systematic errors. However, as demonstrated recently, an analysis incorporating deconvolution of line shapes allows for accurate energy calibration and can provide additional information on kinetics [21–23]. The deconvolution of laser line shape and time profile of a pulse provides the instrument response function, which is the detector signal that would originate from an infinitively short heat input. The time profile determined by the chopper has been analyzed for laser pulses by means of a photo diode. It is a trapezoidal function with a full width at half maximum of 270 ms and total times for the rising and falling edge of 3 ms, i.e. nearly identical to a square wave. Figure 1b shows the instrument response function (blue solid) derived from the laser line shape (red solid). Since the timing for laser and molecular beam pulses is identical, the instrument response can be used to deconvolute the signal for the molecular beam pulse resulting in the heat release relative to the laser power. In particular, comparing the laser signal to the molecular beam signal for water adsorption on CaO(001) at 300 K and at saturation coverage shows strong deviations and the heat signal here is even negative after the end of the pulse time

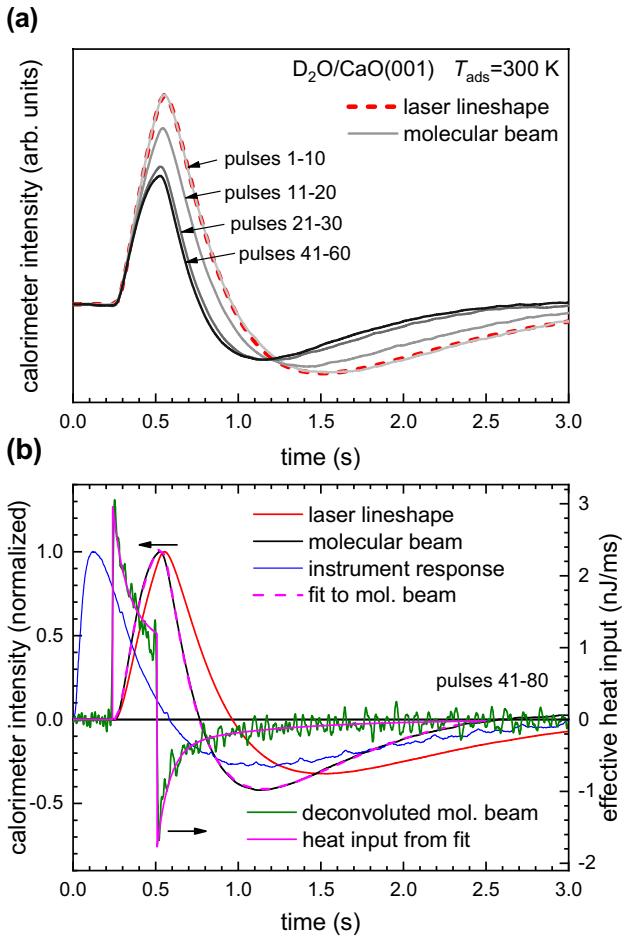

Fig. 1 **a** Averaged calorimetric response from the heat detector for several consecutive sets of molecular pulses of gaseous D_2O on the CaO(001) surface (solid lines) at 300 K. These are compared to the laser pulses on the same surface (dashed line), showing that the molecular pulses narrow with increasing pulse number and coverage. **b** Deconvolution of the heat detector response into its individual components, including the instrument response function (blue solid) from the laser line shape (red solid) and heat released from the molecular pulses (green solid) from the molecular beam pulses (black solid)

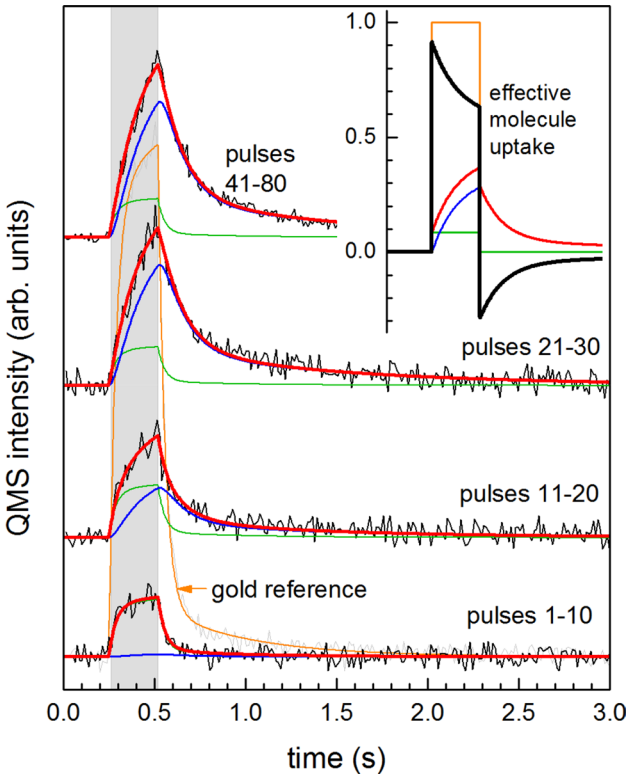

Fig. 2 QMS signal for several consecutive sets of molecular pulses of gaseous D_2O on the CaO(001) surface (black) and the gold reference flag with zero sticking probability (orange). For the deconvolution analysis the latter is analytically expressed by a convolution of a square wave and a double exponential decay which corresponds to the instrument response function (not shown). The sets of pulses were fitted by a linear combination (red) of the gold reference functional (green) and its convolution with two exponential decay functions with different time constants and weighting factors (blue). Inset: Parametrized deconvoluted contributions to the QMS signal for the data set of pulses 41–80 and the resulting effective molecule uptake on the sample (black)

at about 0.5 s (green graph in Fig. 1b). As evidenced by data from the mass spectrometer, desorption of molecules during the pulse time is the origin for this behavior. In the very beginning of the pulse, adsorption induces a relatively high heat release, similar to what is observed for low coverages, where sticking probability is large. With ongoing exposure of the sample to the molecular beam the temporarily increased coverage results in rising desorption of molecules and therefore lowers the total heat deposition. After closure of the chopper only the negative heat contribution of desorbing molecules remains.

During the adsorption experiment, the mass spectrometer records the background pressure for the dosed species. Figure 2 shows the QMS signals for water adsorption on CaO(001) at 300 K averaged for the same pulses as shown in Fig. 1. Initially, the line shape is almost rectangular as it is for the reference measurement on the gold flag placed in front of the sample. With increasing dosage, large intensity can additionally be observed long after the pulse time, which indicates water desorption. The QMS signal for the gold flag is fitted with a square wave convoluted with a superposition of two exponential decay functions, each with different time constants. The resulting gold flag functional (orange in Fig. 2) reflects the response of the vacuum chamber and mass spectrometer for the instrument settings, such as pumping speed or calorimeter temperature, to molecular beam pulses of specific intensity and duration that instantly desorb/reflect with zero-sticking probability. Since the QMS data is relatively noisy and the instrument response function can easily be described by two exponential decay functions instead of explicit deconvolution, we quantify QMS results by fitting analytic expressions. All data sets can be

accurately reproduced by a linear combination (red) of the gold flag functional (green) and its convolution with two further exponential decay functions with different time constants and weighting factors (blue). While the gold flag functional corresponds to a contribution of direct inelastic scattering from the sample the exponential decay functions mimic desorption of first-order reaction processes. The use of a double exponential decay has been previously attributed to desorption of two distinct and independent surface species [26, 27]. Here, it seems to be necessary to properly describe the experimental data. The result from the fit corresponds to the deconvoluted QMS signal. The line shapes for the gold flag functional (orange), the fraction of direct inelastic scattering from the sample (green), the fraction of desorbing molecules (blue) and its superposition (red) are shown in the inset of Fig. 2 for the saturation regime (pulses 41–80). When this parametrized deconvoluted QMS signal is subtracted from the square wave of the incoming molecular beam pulse, an effective molecule uptake on the sample is derived (black graph). It is positive for net adsorption and negative for ongoing desorption after the pulse.

For the determination of the adsorption energy per mole, the measured heat must be referred to the fraction of molecules adsorbed during pulse time, which was denoted as "short-time sticking probability" [16, 28]. In contrast, the "long-time sticking probability" is derived from the total number of desorbed molecules, i.e. from integrated QMS intensity also for the time after the pulse and before the next pulse. Its accumulation multiplied by the number of molecules per pulse provides the surface coverage. Justified by the delay between the heat deposited on the sample and the calorimeter signal, for the determination of short-time sticking probability Lytken et al. weighted the contribution of early and late desorption events within the pulse time linearly between 1 for the beginning and 0 for the end of the pulse [16]. However, as long as the pulse duration is short enough that saturation effects in the detector do not play a role, each adsorption/desorption event (or heat input by laser irradiation) contributes to the calorimeter signal in the same way resulting in a linear slope for a constant heat input. Therefore, assuming a linear slope provides the averaged heat input, which must be related to the total number of sticking molecules within the pulse time. However, when the calorimetry line shape differs for molecular beam and laser pulses, deconvolution analysis of both mass spectrometer data and calorimetry data might provide more accurate results.

To quantify the results from the heat detector, the raw data for the saturation regime was fitted by the convolution of the heat response function (blue in Fig. 1b) with an effective heat input (solid pink graph in Fig. 1b), similar to the method presented by Silbaugh et al.[21] The latter is described by a square wave function for positive heat release for adsorption during the pulse, minus the convolution of square wave and double exponential decay function, which corresponds to removal of heat for increasing desorption for the temporarily enhanced coverage during pulse time. The resulting reconvoluted signal (dashed pink graph) fits perfectly to the experimental data.

For the deconvolution analysis of QMS and calorimetry data, similar but not necessarily identical time constants of the exponential functions were derived. Also, the relative intensity of the two exponential functions, as well as the constant and variable contributions to the effective heat or molecule inputs, differs (compare Figs. 1b and 2 and replicated in the inset of Fig. 3). As a consequence, their ratio (i.e. the adsorption energy per mole) varies within the pulse time. The ratio for the beginning of the result (shaded red) is about 50% larger than the ratio for the end of the pulse (shaded blue).

So far the deconvolution analysis has been described only for the saturation regime averaged for 40 pulses. For the derivation of the effective heat release and molecule uptake profile for each pulse, the number of fitting parameters must be reduced in order to prevent overfitting of the data and consequently artificially scattering fit results. It is assumed that the time constants of the two exponential decay functions (separately for calorimeter and QMS data) as well

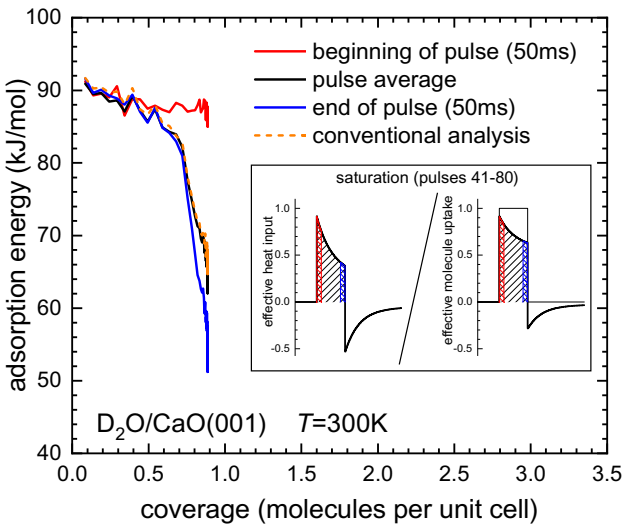

Fig. 3 Adsorption energy for D_2O on the CaO(001) surface on the basis of deconvolution analysis using the beginning, end, and total pulse window over the total pulse time of 270 ms. Each data point corresponds to the evaluation of energy and cumulative long-time sticking for a single pulse (connecting lines for better visibility). Inset: Derived effective heat input from calorimeter signal (left, see also Fig. 1b) and effective molecule uptake from mass spectrometer signal (right, see also Fig. 2) for the saturation regime. Due to their different shape caused by different time constants and relative intensities also differing ratios (i.e. adsorption energies) are obtained for each part of the pulse (shaded areas). Here, we define the CaO(001) unit cell as the number of surface O atoms (8.6×10^{14} atoms per cm^2)

as their relative amount does not change. Aside a variable background from the preceding pulse for each pulse, two parameters are derived which describe the effective heat release or molecule uptake (analogue to inset of Fig. 3 for saturation coverage). These are the intensity of the square wave contribution to the profile (corresponding to a line shape like the laser reference for calorimeter and like gold flag for QMS data) and of the variable, desorption induced contribution with parameters from the saturation regime. For the QMS data the results of this fit procedure are shown in Fig. 2 (summed up for 10 consecutive pulses). With varying intensities of the two contributions (green and blue graph) the data is well reproduced. In view of the larger signal-to-noise ratio for single pulses it is not feasible to also include the three fixed parameters of double exponential decay in the fit. As stated before a single exponential decay function is not sufficient to describe the data. For further examples of this kind of evaluation for different surface temperatures see the Supplementary Information.

In Fig. 3, the adsorption energy per mole is shown for each pulse (with connecting lines for better visibility) as a function of coverage based on the long-time sticking probability from the derived total integral of QMS signal (see following section). The ratio of energy and molecule number is derived from different parts of the pulse. While for the initial 50 ms of the pulse the energy remains constant (red graph), it drops drastically for an evaluation based on the final 50 ms (blue) when desorption starts near saturation coverage. For the integral of the total pulse time the drop is not as pronounced. The dashed orange graph in Fig. 3 shows the result from the conventional analysis for the evaluation of peak heights of the calorimetry signal and the non-weighted short-time sticking probability. It is very close to the deconvolution analysis for the total pulse integral. This demonstrates that the analysis of peak heights provides sufficiently accurate results for the averaged heat release. Before the onset of desorption, all variants of analysis lead to the same adsorption energy, which supports their validity.

4 Results and Discussion

4.1 Water (D_2O) Adsorption

Water adsorption on alkali earth oxides, in general, has been studied extensively in the past, and we refer to a review article[29] for a summary of the most important results. Water adsorption results in dissociated and non-dissociated molecules on the surface, as detected by IRAS[13], which at room temperature and 0.3 L exposure exhibit an interesting structure, where the combination of adsorbed hydroxyl groups and non-dissociated water form linear chains across the surface and along the CaO(110) direction. At higher water exposures the surface starts to disorder and a fully hydroxylated surface approaching a situation as encountered in $Ca(OH)_2$ is created.

Figure 4a shows the sticking probability as a function of coverage, in units of adsorbed molecules per unit cell, measured during the D_2O adsorption microcalorimetry experiments. We define the CaO(001) unit cell as the number of surface O atoms (8.6×10^{14} atoms per cm^2). These results are also presented in terms of dose in Fig. 4b. At all temperatures, the sticking probability is initially constant and near unity [30] until the saturation coverage. This indicates a

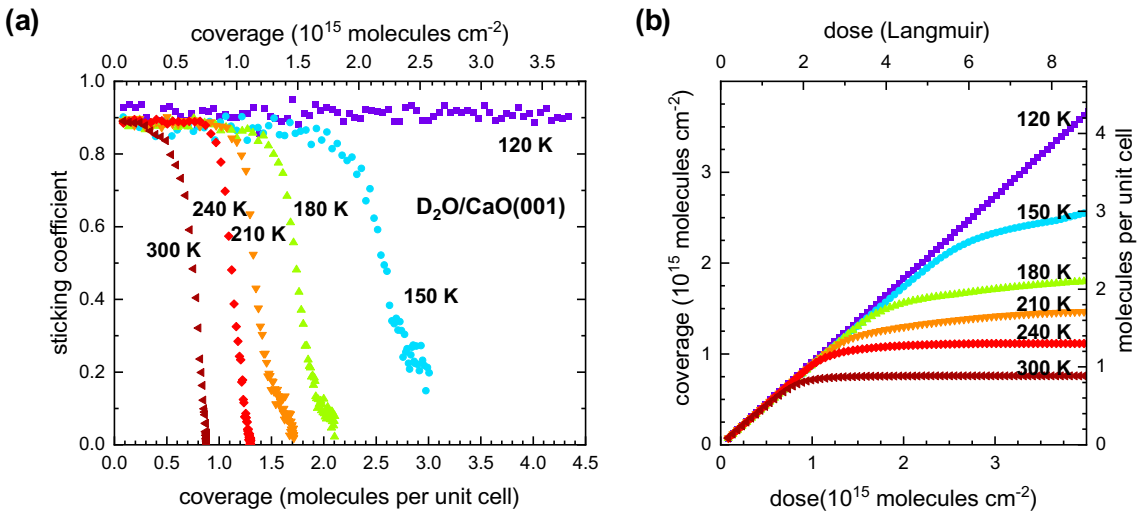

Fig. 4 **a** Sticking coefficient for water adsorption on the CaO(001) surface and **b** resulting dependency of the surface coverage on the molecule dose for different surface temperatures. Each data point corresponds to an individual molecule pulse. The CaO(001) unit cell is defined as the number of surface O atoms (8.6×10^{14} atoms per cm^2)

precursor-mediated adsorption mechanism [31]. At the saturation coverage, the sticking probability rapidly decreases to zero or near zero. The saturation coverage increases with decreasing temperature. At 120 K, water is expected to form multilayer ice [32–36]. As a result, its sticking probability remains constant at 0.9 independent of coverage.

In this paper, the adsorption energies shown are the negative standard difference in internal energy of the system (adsorption energy = $-\Delta U^0$). This internal energy includes two correction terms associated with adsorption and reflection that is detailed by Eqs. 7 and 8 from Lytken et al. [16], but does not include the term associated with pressure–volume work ($\Delta n_{gas} RT_{sample}$) that would convert this internal energy into an enthalpy.

Figure 5 shows the adsorption energies derived from microcalorimetry measurements as a function of coverage in units of adsorbed water molecules per unit cell. For surface temperatures between 120 and 300 K the results from a conventional analysis are compared with the horizontally shifted results from deconvolution analysis taking only the first 50 ms of the pulse time into account. In addition to a larger scattering of data, the latter exhibits significantly higher energies when desorption is relevant close to saturation coverage. The reason might be the temporarily enhanced coverage during molecular beam exposure which increasingly lowers the adsorption energy within the pulse time. Therefore, using the pulse average (by means of complete window integration in deconvolution analysis or by conventional analysis) can give improper results.

The initial adsorption energy of 85–90 kJ/mol is consistent with the previous observations of water dissociation identified by XPS and IRAS [13]. This dissociation occurs at all measured temperatures. At 120 K and when there is a ratio of ~ 3.0 water molecules for every one oxygen atom, water forms multilayer ice. This initial value agrees with the calculated energies between 90 and 110 kJ/mol for the dissociated monomer species [13, 37]. At 300 K, slightly larger initial energies compared to those at lower temperatures are observed. This may be related to formation of one dimensional water chains that were previously observed only at room temperature after doses of about 0.1 L, which corresponds to a coverage of about 0.05 ML [38]. For coverages below 0.8 ML the energy is almost constant for higher temperatures. This indicates ongoing dissociation of water molecules and supports the findings by XPS and IRAS that the surface is fully hydroxylated [13]. In contrast, for low temperatures the energy decreases faster. Here some molecules adsorb at energetically less favorable sites or maybe small clusters with water molecules in the second layer are formed and therefore the average adsorption energy is reduced. IRAS experiments identified different surface species at 100 K and 300 K for low coverages [13].

Above 0.8 ML the energy is significantly reduced. DFT calculations predict that the adsorption energy decreases only slightly from about 110 kJ/mol for a single molecule to 100 kJ/mol for one monolayer coverage [13]. However, the latter value represents the average adsorption energy for all molecules in the considered 4 × 3 unit cell, so it can be expected that the differential adsorption energy for the last molecule to complete the monolayer is considerably lower. This is most likely related to the increase in the fraction of molecularly adsorbed water as derived from the structural models which was also observed in XPS spectra [13]. Therefore, aggregate formation will further decrease the average energy.

For temperatures above 120 K, the energy levels off when the individual saturation coverage is reached. Below saturation the adsorption energy is comparable for all temperatures

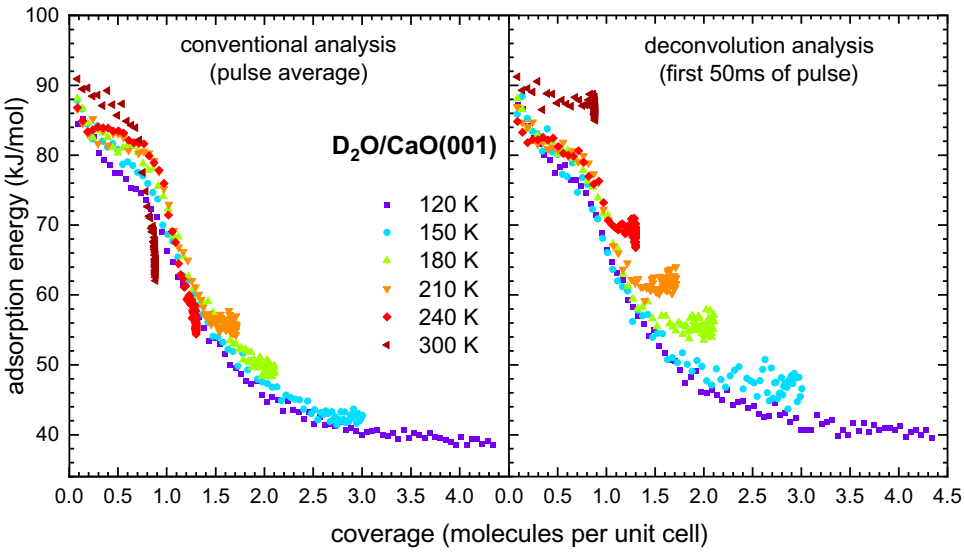

Fig. 5 Adsorption energy from microcalorimetry using the conventional analysis i.e. average for the entire pulse time of 270 ms (left panel) and for the first 50 ms via deconvolution of calorimetry and QMS data (right panel) for sample temperatures as indicated. Each data point corresponds to an individual molecule pulse. The CaO(001) unit cell is defined as the number of surface O atoms (8.6×10^{14} atoms per cm^2)

except for 300 K as discussed above. At 120 K, multilayer formation with an adsorption energy of ~40 kJ/mol is observed. This slightly deviates from the previously measured heats of multilayer adsorption of D_2O on Pt(111) and Ni(111), 47 kJ/mol [20, 32], and on Fe_3O_4(111)/Pt(111) and FeO(111)/Pt(111) films, 45 kJ/mol. [39] However, previous work [29] has revealed a complication where high doses of water cause a dissolution of the CaO substrate surface. This creates difficulties accurately measuring the multilayer adsorption energies. Unfortunately, the time scales of this process is unknown, and therefore further studies are necessary.

In the next experiments, we addressed the possible role of surface defects on the water adsorption energy. For this, we artificially created defects by bombardment of the well prepared CaO(001) film with 2 keV Ar^+ ions and subsequently performed microcalorimetry measurements (Fig. 6). Compared to the "as grown" surface, the initial adsorption energy is enhanced by a factor of 2. With increasing water dosage the energy drops rapidly and finally reaches similar values as the ordered surface. After the sample was heated in UHV to 1100 K, a second calorimetry measurement still reveals an enhanced initial adsorption energy of about 120 kJ/mol, but already after about 0.4 L of water the energy is identical to that for the ordered surface. Annealing at 1300 K seems to heal all defects and the adsorption energy curve reproduces that of the well-ordered film. These results indicate that water preferentially adsorbs on surface defects presumably involving higher coordinated sites, and once all sites are occupied, the adsorption energy is not affected by the still present enhanced surface roughness. However, for the well-ordered CaO(001) surface, small amounts of defect sites (<0.1 mL) might be present but would be efficiently populated by water molecules from the residual gas before the first pulse of the molecular beam. Furthermore, this is complicated by the possibility of CaO (and other alkaline earth oxides) restructuring to form $Ca(OH)_2$, a process that may be expedited by surface defects [40].

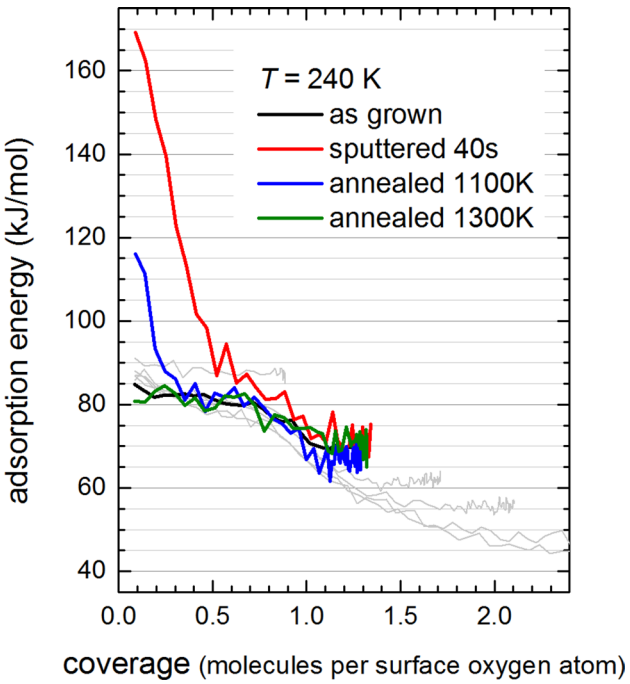

Fig. 6 Adsorption energy of D_2O on the CaO(001) surface for sputter-induced surface defects based on deconvolution analysis using the initial 50 ms of the pulse time. The CaO(001) unit cell is defined as the number of surface O atoms (8.6×10^{14} atoms per cm^2). Each data point corresponds to an individual molecule pulse (connecting lines for better visibility)

4.2 CO_2 Adsorption

The interaction of CO_2 with a CaO(100) has been studied in the past via TPD, IRAS, and DFT [41, 42]. Recently, we have also investigated the interaction of CO_2 and water on a CaO(100) surface using the above mentioned experimental techniques [25].

Figure 7a shows the sticking probability as a function of coverage, in units of adsorbed CO_2 molecules per unit cell, measured during microcalorimetry experiments. These results are also presented in terms of dose in Fig. 7b. Similar to water, the sticking coefficient is constant for low coverages. This points to a precursor-mediated adsorption process, which is also supported by DFT calculations where a stable physisorbed surface state was derived [12]. Note that all of the measured temperatures are higher than the temperature limit where multilayer growth is expected to occur [10]. Therefore, CO_2 reaches a saturation coverage at all temperatures studied.

The relatively high initial adsorption energy of about 125 kJ/mol indicates strong chemical interaction of carbon dioxide with the surface (Fig. 8). For all studied temperatures the trend of energies is similar. Up to about 0.3 mL coverage, the energy continuously decreases to about 75% of the initial energy and then drops to energies in the regime of physisorption. For low temperatures the sticking probability is still high, whereas for room temperature saturation is reached already at about 0.4 mL coverage after a dose of about 2 L CO_2. These results are consistent with TPD, which gives heat of adsorption at low coverages of 120–140 kJ/mol [12].

From our previous IRAS and DFT study, formation of monodentate carbonate species was concluded [12]. These experiments observed several different vibrational frequencies with increasing dose, indicating different adsorption sites. For the lowest dose of 0.1 L, the full population of step edges with adsorption energies of up to 300 kJ/mol was assumed. For higher coverages the calculated frequencies for the models with aggregates of two and three

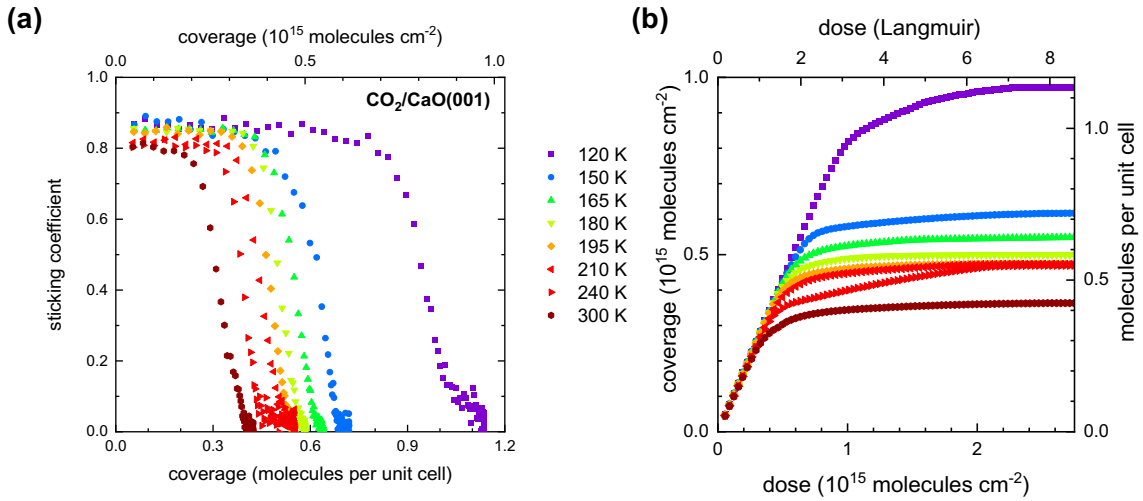

Fig. 7 **a** Sticking coefficient for CO_2 adsorption on CaO(001) and **b** resulting dependency of the surface coverage on the molecule dose for different surface temperatures. The CaO(001) unit cell is defined as the number of surface O atoms (8.6×10^{14} atoms per cm^2)

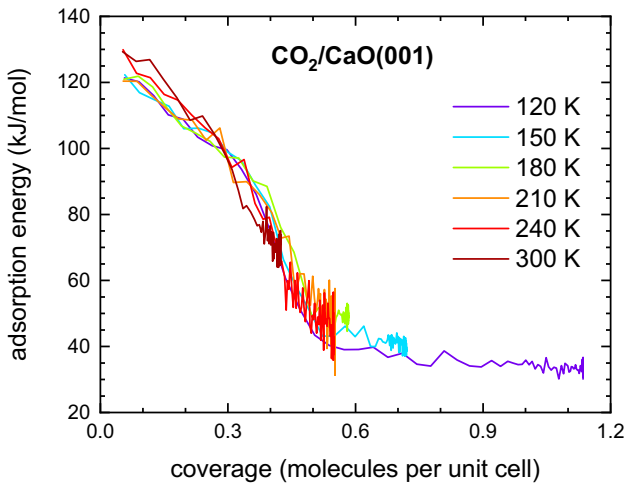

Fig. 8 Adsorption energy from microcalorimetry for CO_2 adsorption on the CaO(001) surface incorporating deconvolution of calorimetry and QMS data (initial 50 ms of pulse time). The CaO(001) unit cell is defined as the number of surface O atoms (8.6×10^{14} atoms per cm^2). Each data point corresponds to an individual molecule pulse (connecting lines for better visibility)

molecules with same orientation fit to the experimental spectra. Also, the decreasing adsorption energies for coverages up to one third of a monolayer indicate lateral interaction of surface species and formation of small carbonate clusters. The calculated energies are considerably larger, but also continuously decrease with cluster size from about 185 kJ/mol to 150 kJ/mol. For higher coverages additional peaks in the vibrational spectra can be explained by the arrangement of molecules rotated by 90°. Then, also the calculated adsorption energies are considerably reduced. This may be an explanation for the drop in the adsorption energy derived from microcalorimetry at a coverage of about 0.3 mL. A coverage of a third of a monolayer might also be the limit for parallel chains of carbonate species without significant interaction between neighboring rows. If the temperature is low enough to allow for larger coverages, diagonal stripes with a different orientation intersect resulting in the reduction of adsorption energy.

To better understand the interaction between water and CO_2 adsorbed on the surface, clean CaO(001) was predosed with varying exposures of water before proceeding with microcalorimetry experiments of CO_2 adsorption. Figure 9a shows the sticking probability as a function of coverage, in units of adsorbed CO_2 molecules per unit cell, measured during microcalorimetry experiments. For all exposures of water up to 1.8 L, the initial sticking probability is ~0.85 and remains constant until the saturation coverage is reached. This saturation coverage decreases with increasing water dose. At higher water doses, the initial sticking probability decreases, and is about 0.3 with 9.6 L water. Figure 9b shows the adsorption energies derived from microcalorimetry measurements as a function of coverage in units of adsorbed CO_2 molecules per unit cell. With higher pre-doses of water, the initial measured heats of adsorption decrease. However, the heats of adsorption of CO_2 on CaO(001) predosed with 0–1.8 L water decrease with coverage at a similar rate, and all approach the same value (~40 kJ/mol). This suggests that water blocks adsorption sites, lowering the saturation coverage, and produces steric repulsions with the adsorbing CO_2, thereby lowering the adsorption energy. Indeed, these adsorption energies would match the clean surface if each curve was shifted directly right on Fig. 9b, as if the curves started at non-zero coverages, with higher

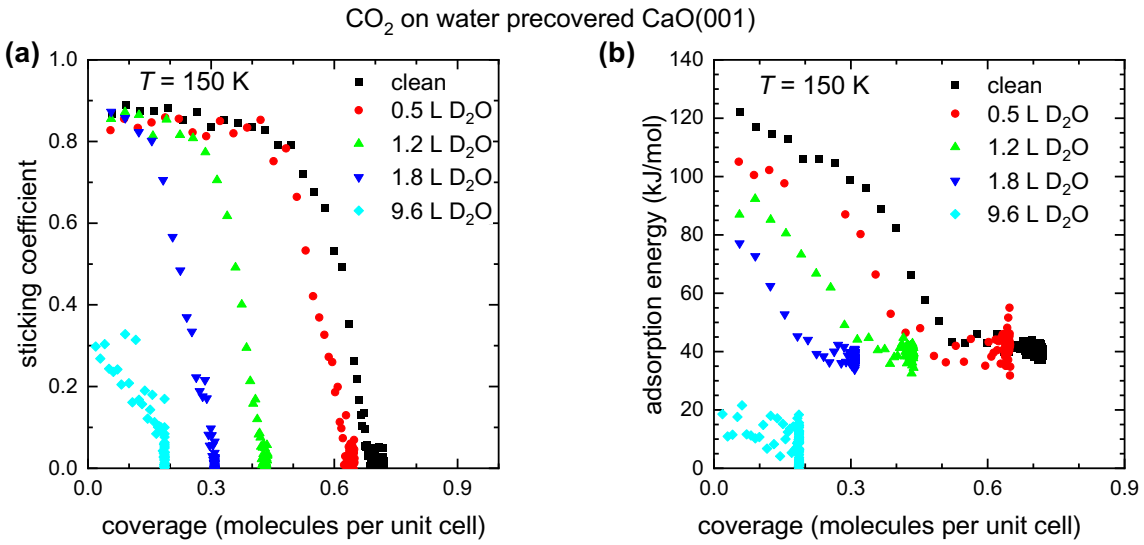

Fig. 9 Sticking coefficient (**a**) and adsorption energy (**b**) for carbon dioxide adsorption on water covered CaO(001) surface after the indicated water dosages. The adsorption energy is based on deconvolution analysis using the initial 50 ms of the pulse time. The CaO(001) unit cell is defined as the number of surface O atoms (8.6×10^{14} atoms per cm^2)

pre-doses of water causing the CO_2 adsorption energy curves to start at higher coverages.

5 Conclusions

A new method of analysis was employed to deconvolute the line shapes of the heat detector response into the instrument response function, two exponential decay functions, that correspond to the desorption of two distinct surface species. This method allows for a thorough analysis of the adsorption, dissociation, and desorption processes that occur during our microcalorimetry experiments.

This analysis method has been applied to study the interactions of D_2O and CO_2 on CaO(001) thin films using microcalorimetry. D_2O adsorbs initially with an adsorption energy of 85–90 kJ/mol at temperatures ranging from 120 to 300 K, consistent with prior spectroscopic studies that indicate dissociation. This adsorption energy decreases with increasing coverage until either multilayers are formed at low temperatures (120 K) or the surface is saturated (> 150 K). Artificially producing defects on the surface by sputtering beforehand increases this energy.

CO_2 adsorbs on CaO(001) with an initial adsorption energy of ~ 125 kJ/mol, and continually decreases until the saturation coverage is reached. This total CO_2 coverage decreases with increasing temperature. To understand the surface interactions of CO_2 and water, the CaO(001) surface was predosed with water preceding CO_2 microcalorimetry experiments. We find that water blocks adsorption sites, lowers the saturation coverage, and lowers the measured adsorption energy.

The calorimetry data shown here further adds to our understanding of D_2O and CO_2 adsorption on the CaO(001) surface, building on previous studies that had IRAS, STM, and TPD, in combination with DFT calculations [11–13]. However, this previous work was primarily focused on lower coverages (i.e., less than one monolayer). Caution must be exercised when expanding this work to higher coverages, where multilayers of water tend to dissolve surface Ca resulting in a complete restructuring of the surface [40].

Supplementary Information The online version contains supplementary material available at https://doi.org/10.1007/s11244-021-01431-2.

Funding Open Access funding enabled and organized by Projekt DEAL.

References

1. Freund H-J, Roberts MW (1996) Surface chemistry of carbon dioxide. Surf Sci Rep 25:225–273
2. Burghaus U (2009) Surface science perspective of carbon dioxide chemistry-Adsorption kinetics and dynamics of CO_2 on selected model surfaces. Cat Today 148:212–220. https://doi.org/10.1016/j.cattod.2009.07.082
3. Choi S, Drese JH, Jones CW (2009) Adsorbent materials for carbon dioxide capture from large anthropogenic point sources. Chemsuschem 2:796–854. https://doi.org/10.1002/cssc.200900036
4. Grabow LC, Mavrikakis M (2011) Mechanism of methanol synthesis on Cu through CO_2 and CO hydrogenation. ACS Catal 1:365–384. https://doi.org/10.1021/cs200055d
5. Taifan W, Boily J-F, Baltrusaitis J (2016) Surface chemistry of carbon dioxide revisited. Surf Sci Rep 71:595–671. https://doi.org/10.1016/j.surfrep.2016.09.001
6. Mandal SPSK (2020) From CO_2 activation to catalytic reduction: a metal-free approach. Chem. Sci. 11:10571–10593. https://doi.org/10.1039/D0SC03528A
7. Quadrelli EA, Centi G, Duplan J-L, Perathoner S (2011) Carbon dioxide recycling: emerging large-scale technologies with industrial potential. Chemsuschem 4:1194–1215. https://doi.org/10.1002/cssc.201100473
8. Klankermayer J, Wesselbaum S, Beydoun K, Leitner W (2016) Selective catalytic synthesis using the combination of carbon dioxide and hydrogen: catalytic chess at the interface of energy and chemistry. Angew Chem Int Ed 55:7296–7343. https://doi.org/10.1002/anie.201507458
9. Chinchen GC, Denny PJ, Parker DG, Spencer MS, Whan DA (1987) Mechanism of methanol synthesis from CO_2/CO/H_2 mixtures over copper/zinc oxide/alumina catalysts: use of ^{14}C-labelled reactants. Appl Catal 30:333–338. https://doi.org/10.1016/S0166-9834(00)84123-8
10. Kadossov E, Burghaus U (2008) Adsorption kinetics and dynamics of CO, NO, and CO_2 on reduced CaO(100). J Phys Chem C 112:7390–7400. https://doi.org/10.1021/jp800755q
11. Solis BH, Sauer J, Cui Y, Shaikhutdinov S, Freund H-J (2017) Oxygen scrambling of CO_2 adsorbed on CaO(001). J Phys Chem C 121:18625–18634. https://doi.org/10.1021/acs.jpcc.7b05293
12. Solis BH, Cui Y, Weng X, Seifert J, Schauermann S, Sauer J, Shaikhutdinov S, Freund H-J (2017) Initial stages of CO_2 adsorption on CaO: a combined experimental and computational study. Phys Chem Chem Phys 19:4231–4242. https://doi.org/10.1039/C6CP08504K
13. Fujimori Y, Zhao X, Shao X, Levchenko SV, Nilius N, Sterrer M, Freund H-J (2016) Interaction of Water with the CaO(001) Surface. J Phys Chem C 120:5565–5576. https://doi.org/10.1021/acs.jpcc.6b00433
14. Campbell CT (2019) Energies of adsorbed catalytic intermediates on transition metal surfaces: calorimetric measurements and benchmarks for theory. Acc Chem Res 52:984–993. https://doi.org/10.1021/acs.accounts.8b00579
15. Schauermann S, Silbaugh TL, Campbell CT (2014) Single-crystal adsorption calorimetry on well-defined surfaces: from single crystals to supported nanoparticles. Chem Rec 14:759–774. https://doi.org/10.1002/tcr.201402022
16. Lytken O, Lew W, Harris JJW, Vestergaard EK, Gottfried JM, Campbell CT (2008) Energetics of cyclohexene adsorption and reaction on Pt(111) by low-temperature microcalorimetry. J Am Chem Soc 130:10247–10257. https://doi.org/10.1021/ja801856s
17. Borroni-Bird CE, Al-Sarraf N, Andersoon S, King DA (1991) Single crystal adsorption microcalorimetry. Chem Phys Lett 183:516–520. https://doi.org/10.1016/0009-2614(91)80168-W
18. Stuckless JT, Frei NA, Campbell CT (1998) A novel single-crystal adsorption calorimeter and additions for determining metal adsorption and adhesion energies. Rev Sci Instrum 69:2427–2438. https://doi.org/10.1063/1.1148971
19. Fischer-Wolfarth J-H, Hartmann J, Farmer JA, Flores-Camacho JM, Campbell CT, Schauermann S, Freund H-J (2011) An improved single crystal adsorption calorimeter for determining gas adsorption and reaction energies on complex model catalysts. Rev Sci Instrum 82:024102. https://doi.org/10.1063/1.3544020
20. Lew W, Crowe MC, Karp E, Campbell CT (2011) Energy of molecularly adsorbed water on clean Pt(111) and Pt(111) with coadsorbed oxygen by calorimetry. J Phys Chem C 115:9164–9170. https://doi.org/10.1021/jp201608x
21. Silbaugh TL, Karp EM, Campbell CT (2013) Surface kinetics and energetics from single crystal adsorption calorimetry lineshape analysis: Methyl from methyl iodide on Pt(111). J Catal 308:114–121. https://doi.org/10.1016/j.jcat.2013.05.030
22. Silbaugh TL, Karp EM, Campbell CT (2014) Energetics of formic acid conversion to adsorbed formates on Pt(111) by transient calorimetry. J Am Chem Soc 136:3964–3971. https://doi.org/10.1021/ja412878u
23. Wolcott CA, Campbell CT (2015) Method for direct deconvolution of heat signals in transient adsorption calorimetry. Surf Sci 633:17–23. https://doi.org/10.1016/j.susc.2014.11.005
24. King DA, Wells MG (1972) Molecular beam investigation of adsorption kinetics on bulk metal targets: nitrogen on tungsten. Surf Sci 29:454–482. https://doi.org/10.1016/0039-6028(72)90232-4
25. Weng X, Cui Y, Shaikhutdinov S, Freund H-J (2019) CO2 Adsorption on CaO(001): temperature-programmed desorption and infrared study. J Phys Chem C 123:1880–1887. https://doi.org/10.1021/acs.jpcc.8b11415
26. Ihm H, Ajo HM, Gottfried JM, Bera P, Campbell CT (2004) Calorimetric measurement of the heat of adsorption of benzene on Pt(111). J Phys Chem B 108:14627–14633. https://doi.org/10.1021/jp040159o
27. Starr DE, Campbell CT (2008) Large entropy difference between terrace and step sites on surfaces. J Am Chem Soc 130:7321–7327. https://doi.org/10.1021/ja077540h
28. Flores-Camacho JM, Fischer-Wolfarth JH, Peter M, Campbell CT, Schauermann S, Freund HJ (2011) Adsorption energetics of CO on supported Pd nanoparticles as a function of particle size by single crystal microcalorimetry. Phys Chem Chem Phys 13:16800–16810. https://doi.org/10.1039/C1CP21677E
29. Sterrer M, Nilius N, Shaikhutdinov S, Heyde M, Schmidt T, Freund H-J (2019) Interaction of water with oxide thin film model systems. J Mater Res 34:360–378. https://doi.org/10.1557/jmr.2018.454
30. Kisliuk P (1957) The sticking probabilities of gases chemisorbed on the surfaces of solids. J Phys Chem Solids 3:95–101. https://doi.org/10.1016/0022-3697(57)90054-9
31. Lombardo SJ, Bell AT (1991) A review of theoretical models of adsorption, diffusion, desorption, and reaction of gases on metal surfaces. Surf Sci Rep 13:3–72. https://doi.org/10.1016/0167-5729(91)90004-H
32. Zhao W, Carey SJ, Mao Z, Campbell CT (2018) Adsorbed hydroxyl and water on Ni(111): heats of formation by calorimetry. ACS Catal 8:1485–1489. https://doi.org/10.1021/acscatal.7b04041
33. Dauenhauer PJ, Abdelrahman OA (2018) A universal descriptor for the entropy of adsorbed molecules in confined spaces. ACS Cent Sci 4:1235–1243. https://doi.org/10.1021/acscentsci.8b00419
34. Lustemberg PG, Palomino RM, Gutiérrez RA, Grinter DC, Vorokhta M, Liu Z, Ramírez PJ, Matolín V, Ganduglia-Pirovano MV, Senanayake SD, Rodriguez JA (2018) Direct conversion of

methane to methanol on Ni-ceria surfaces: metal-support interactions and water-enabled catalytic conversion by site blocking. J Am Chem Soc 140:7681–7687. https://doi.org/10.1021/jacs.8b03809
35. Carey SJ, Zhao W, Campbell CT (2018) Bond energies of adsorbed intermediates to metal surfaces: correlation with hydrogen-ligand and hydrogen-surface bond energies and electronegativities. Angew Chem Int Ed 57:16877–16881. https://doi.org/10.1002/anie.201811225
36. McBride F, Hodgson A (2018) The reactivity of water and OH on Pt–Ni(111) films. Phys Chem Chem Phys 20:16743–16748. https://doi.org/10.1039/C8CP01205A
37. Hu XL, Carrasco J, Klimeš J, Michaelides A (2011) Trends in water monomer adsorption and dissociation on flat insulating surfaces. Phys Chem Chem Phys 13:12447–12453. https://doi.org/10.1039/C1CP20846B
38. Zhao X, Shao X, Fujimori Y, Bhattacharya S, Ghiringhelli LM, Freund H-J, Sterrer M, Nilius N, Levchenko SV (2015) Formation of water chains on CaO(001): what drives the 1D growth? J Phys Chem Lett 6:1204–1208. https://doi.org/10.1021/acs.jpclett.5b00223
39. Dementyev P, Dostert K-H, Ivars-Barceló F, O'Brien CP, Mirabella F, Schauermann S, Li X, Paier J, Sauer J, Freund H-J (2015) Water interaction with iron oxides. Angew Chem Int Ed 54:13942–13946. https://doi.org/10.1002/anie.201506439
40. Ončák M, Włodarczyk R, Sauer J (2015) Water on the MgO(001) surface: surface reconstruction and ion solvation. J Phys Chem Lett 6:2310–2314. https://doi.org/10.1021/acs.jpclett.5b00885
41. Bhatia SK, Perlmutter DD (1983) Effect of the product layer on the kinetics of the CO2-lime reaction. AIChE J 29:79–86. https://doi.org/10.1002/aic.690290111
42. Yasuo F, Kozo T (1973) Infrared study of carbon dioxide adsorbed on magnesium and calcium oxides. Bull Chem Soc Jpn 46:1616–1619. https://doi.org/10.1246/bcsj.46.1616